LAWRENCE
LIVERMORE
NATIONAL
LABORATORY

LLNL-JRNL-644274

Light-Directed Electrophoretic Deposition: A New Additive Manufacturing Technique for Arbitrarily Patterned 3D Composites

A. J. Pascall, F. Qian, G. Wang, M. A. Worsley, Y. Li, J. D. Kuntz

September 26, 2013

Advanced Materials

Disclaimer

Light-Directed Electrophoretic Deposition: A New Additive Manufacturing Technique for Arbitrarily Patterned 3D Composites

Andrew J. Pascall*, Fang Qian, Gongming Wang, Marcus A. Worsley, Yat Li, Joshua D. Kuntz

Dr. A. J. Pascall, Dr. F. Qian, Dr. M. A. Worsley, Dr. J. D. Kuntz
Lawrence Livermore National Laboratory
Livermore, CA 94550, USA

G. Wang, Prof. Y. Li
Department of Chemistry and Biochemistry
University of California
Santa Cruz, CA 95064, USA

Correspondence to: Dr. A. J. Pascall (E-mail: pascall1@llnl.gov)
This manuscript published as: *Advanced Materials*, Vol. 26(14), 2252-2256

Abstract

A versatile, new additive manufacturing technique based on electrophoretic deposition of colloids onto light patterned photoelectrodes is demonstrated. Particles to be deposited move via electrophoresis and adhere to the illuminated regions of the electrode. This process is repeated with different materials and illumination patterns to fabricate arbitrarily patterned 3D multimaterial composites.

Keywords: EPD, additive manufacturing, multimaterial, virtual electrodes, 3D printing

Electrophoretic deposition (EPD) is a process in which electrically charged colloids are forced to deposit onto the surface of an electrode due to an electric field. EPD was originally developed nearly a century ago for applying paint to metal surfaces.[1] Since then, EPD has been used to deposit a wide range of materials on conductive surfaces including ceramics,[2] metals,[3] polymers,[4] living cells,[5, 6] and biological material.[7] EPD allows exquisite control over layer thickness and gradients of materials normal to the surface[8] and has been employed to conformally coat complex 3D electrodes[9] and as a near net shape manufacturing technique[10]. EPD has proven useful in applications as diverse as barrier coatings,[11] medical implants,[12] energetic materials,[13] chemical sensors,[14, 15] energy storage,[16, 17] solar cells,[18, 19] and solid state lighting.[20]

One major drawback of traditional EPD, however, is that gradients in deposit composition can only be realized in a direction normal to the electrode surface. This is because the electrode geometry is generally fixed and cannot be changed during the course of a deposition. Some attempts have been made to create a movable counter electrode to deposit material in a specific location; however, this technique has not demonstrated multimaterial patterning and is difficult to scale.[21, 22]

In this article, we introduce and demonstrate a technique called "light-directed electrophoretic deposition" which uses photoconductive electrodes and DC electric fields to dynamically pattern the electrode during deposition. This allows for the generation of arbitrarily patterned 3D multimaterial composites. The key difference between this technique and traditional EPD is that, with light-directed EPD, the electrode pattern is reconfigurable during the course of an experiment by changing the pattern of illumination on the photoconductive electrode. This allows multiple materials to be placed in arbitrary locations over large areas with fine resolution.

While several authors have utilized a combination of illumination and electric fields to manipulate particles or form patterned deposits from collections of particles, nearly universally, these methods rely on AC electric fields and the particles are manipulated through dielectrophoresis, as with optoelectronic tweezers,[23, 24,

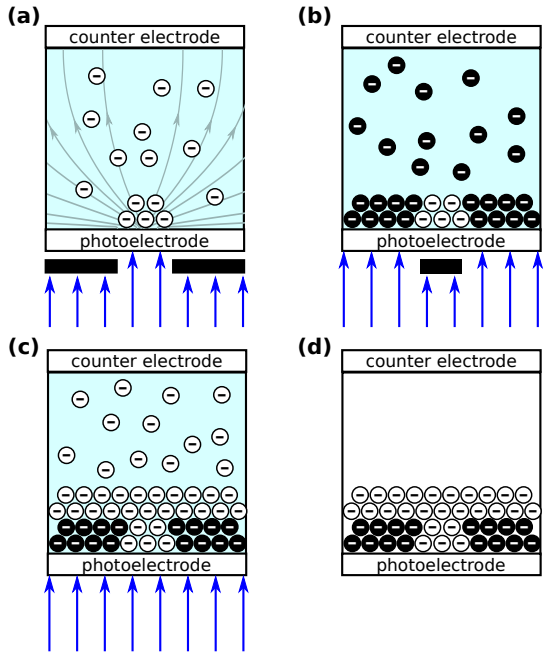

Figure 1: Light-directed electrophoretic deposition scheme. (a) The photoconductive electrode is illuminated (arrows) from the backside through a mask. The conductivity of the illuminated TiO_2 layer increases causing the electric field to concentrate in the illuminated region. Particles (white) in the bulk suspension follow the electric field lines and adhere to the illuminated region of the electrode. (b) The mask pattern and suspension can be changed to deposit another material (black) in a different location. (c) The process can be repeated to place one material on top of another. (d) The suspension can be withdrawn yielding an arbitrarily patterned 3D composite.

25] or electrohydrodynamic flows.[26] Perhaps the closest technique to light-directed EPD described in the literature is the report of Hayward, *et al.*[27] on the assembly of 2D patterned colloidal crystals using DC fields and UV light, but the method of action points to near-surface electrohydrodynamic flows,[28] which limits the ability to form thick 3D deposits. To our knowledge, there have been no reports that demonstrate fabrication of 3D patterned multimaterial composites using DC electric fields.

Light-directed EPD has the potential to elevate EPD from its traditional role as a coating process to a true additive manufacturing technique. By automating the fluid handling and light delivery systems, light-directed EPD will allow rapid patterning of multiple materials over large areas and can produce composites to near net shape from a diverse set of materials, including metals, ceramics, polymers, and biological materials. Controlled voids can also be incorporated into the composite by utilizing a fugitive material that is removed with subsequent post-processing. These capabilities are unique among current additive manufacturing processes.[29]

A typical multimaterial light-directed EPD process is depicted in **Figure 1**. The space between the photoconductive electrode and counter electrode is filled with a suspension of particles that will be deposited. The photoconductive electrode consists of a photoconductive layer of titania nanorods hydrothermally grown on an fluorine doped tin oxide (FTO) coated glass substrate. A photomask is placed on the back side of the photoconductive electrode and illuminated with a light source. An electrical potential difference is imposed between the FTO layer of the photoconductive electrode and the counter electrode. In the regions illuminated by the light source defined by the clear regions of the photomask, the conductivity of the photoconductive film increases. Electric field lines are concentrated in these regions and particles in suspension move long the field lines and attach to the surface of the electrode forming a deposit (Figure 1(a)). The suspension composition and the photomask pattern can be changed to deposit another material in a different location within the same layer (Figure 1(b)). The process can be repeated to build subsequent layers to form an arbitrarily patterned 3D composite (Figure 1(c)). Finally, the suspension can be removed from the chamber yielding a dry deposit while retaining the precise patterning.

The titania nanowire photoconductive electrodes were grown by a hydrothermal method based on previ-

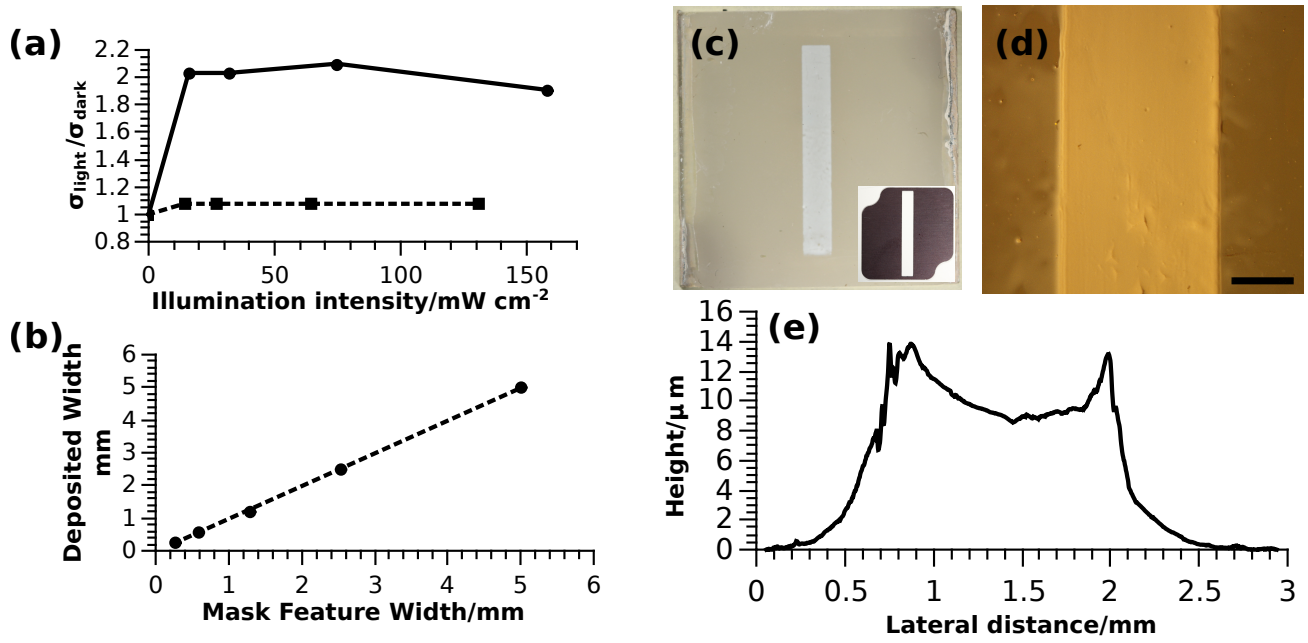

Figure 2: (a) Relative electrode conductivity versus illumination with λ >400 nm (•, solid) and λ >435 nm (■, dashed) wavelength light. (b) Feature size reproduction of the technique with mask feature widths ranging from 0.25 to 5 mm. Least squares regression of the data (dashed) yields a slope of 1.00 ± 0.01 and an intercept of -0.024 ± 0.030 mm with an $R^2 = 0.999$. (c) Photograph of a 2.5 mm wide feature deposited using light-directed EPD. INSET: 2.5 mm mask used to fabricate deposit. (d) Micrograph of the deposit. Scale bar represents 1 mm. (e) A line scan height profile across the 1.25 mm feature's width reveals that it is approximately 9 microns thick at the center and 14 microns thick at the edges. The origin of increased thickness of the edges is described in Ref. [30].

ously published procedures.[31, 32]. Details of the synthesis are presented in the supporting information. In order to determine the photoconductive response of the electrodes, an square of conductive Cu-Ni tape (8 mm on a side, Ted Pella) was affixed to the titania nanowire surface. The backside of the electrode was masked off such that only an area corresponding to the location of the Cu-Ni tape was illuminated. Electrical contact was made both to the underlying FTO layer as well as to the Cu-Ni tape using an electrical probe station. A two-point resistance measurement was conducted using a digital multimeter (2400, Keithley) under various levels of illumination from a mercury arc lamp (X-cite 120Q, Lumen Dynamics). Several long pass filters were inserted in sequence between the light source and electrode to study the effects of illumination wavelength on photoconductivity. **Figure 2**(a) displays the conductivity for illumination with a $\lambda > 400$ nm (circles) and $\lambda > 435$ nm (squares) long pass filter relative to the dark conductivity. Transmission spectra of the filters used are presented in the supporting information. With $\lambda > 400$ nm light, the conductivity increases by a factor of roughly 2 under illumination and remains constant over the range of illumination intensities tested. In contrast, illumination with $\lambda > 435$ nm light barely increases under illumination. This result is consistent with excitation of carriers into the conduction band since titania (rutile phase) has a band gap energy corresponding to $\lambda = 405$ nm.[33]

The light-directed electrophoretic deposition experiments were conducted in a purpose-built cell consisting of two halves machined in Delrin that are assembled to form a solvent tight chamber. The purpose of the cell is to provide optical access to the back side of the deposition electrode, to ensure that the electrodes are parallel and at a fixed spacing, as well as to contain the colloidal suspension and allow rapid exchange of the suspension for multimaterial deposition. In one half of the cell, a liquid flow channel (25 mm wide, 80 mm long, and 250 microns deep) was machined along with fluid ports that allow the channel to accept fluid from external tubing. At the center of the flow channel, a recess was machined to accept the ITO coated glass slide (25 mm square, 1.1 mm thick, Sheet resistance: 8-12 $\Omega\ \square^{-1}$, Sigma-Aldrich) counter electrode. Similarly, in the other half, an identical recess was machined to accept the deposition electrode. Furthermore, a roughly square aperture (22 mm on a side) was milled through the recess to provide optical access to the back side of the deposition electrode. When the cell is assembled, the electrodes sit in their respective recesses opposed across the flow channel such that their top surfaces are flush with the walls of the channel. The gap between the electrodes is set to 250 μm via a set of plastic spacers. Electrical contact is provided through the cell to the back side of electrodes with spring loaded electrodes.

Electrophoretic deposition was performed with the cell in a vertical orientation. That is, the flow axis was oriented parallel to gravity. The suspensions used were either 1 vol% submicron alumina in a solvent composed of 75 vol% ethanol, 25 vol% deionized water, with 0.04 vol% Darvan 821A surfactant added, which yields a white deposit, or a 2 vol% nanoscale tungsten in 100% ethanol with 0.25 vol% Darvan 821A, which yields the black deposit. Both suspensions displayed a negative zeta potential. The details of the suspension preparation and characterization are presented in the supporting information. The cell was loaded with suspension through the bottom port until suspension was seen exiting the top port. Unless otherwise noted, the back side of the photoconductive electrode was illuminated with the full spectrum of a mercury arc lamp at approximately 30 mW/cm^2 through a laser cut aluminum mask. See supplemental figure S1 for spectrum. Depositions were carried out for 30 seconds by applying +2 V_{DC} to the photoconductive electrode with respect to the counter electrode. After 30 seconds, a potential of +1 V_{DC} was held on the electrode during withdrawal of the suspension at 0.25 mL/min. While deposition of material was not observed when applying +1 V_{DC}, the deposited film had better adhesion to the electrode during withdrawal of the suspension. The application of a potential during withdrawal is not a typically employed by the EPD community, but it is not without precedent[34, 35]. After complete withdrawal of the suspension, the deposition electrode was removed and allowed to air dry.

Initial experiments focused on determining under which illumination conditions a deposit would form. To that end, a series of experiments was conducted in which long pass filters were inserted between the mercury arc lamp and electrode. The illumination intensity was held at 25 mW cm^{-2} consistently throughout by inserting neutral density filters and measuring the intensity with a power meter (thermal, ThorLabs). Consistent with the observation that the conductivity of the electrode increases under illumination with λ <400 nm light, no deposit was observed when long pass filters with band edges greater than 400 nm were employed. However, a deposit did form when long pass filters with band edges less than 400 nm were employed. Additionally, a deposit was formed when the photoelectrode was illuminated with a narrowband light emitting diode (LED) at 405 nm (see supplemental figure S1 for spectrum). However, no deposit was observed under illumination with either the mercury arc lamp or LED when the photoconductive electrode was replaced by a bare FTO-on-glass electrode (no photoconductive titania film). We also determined that

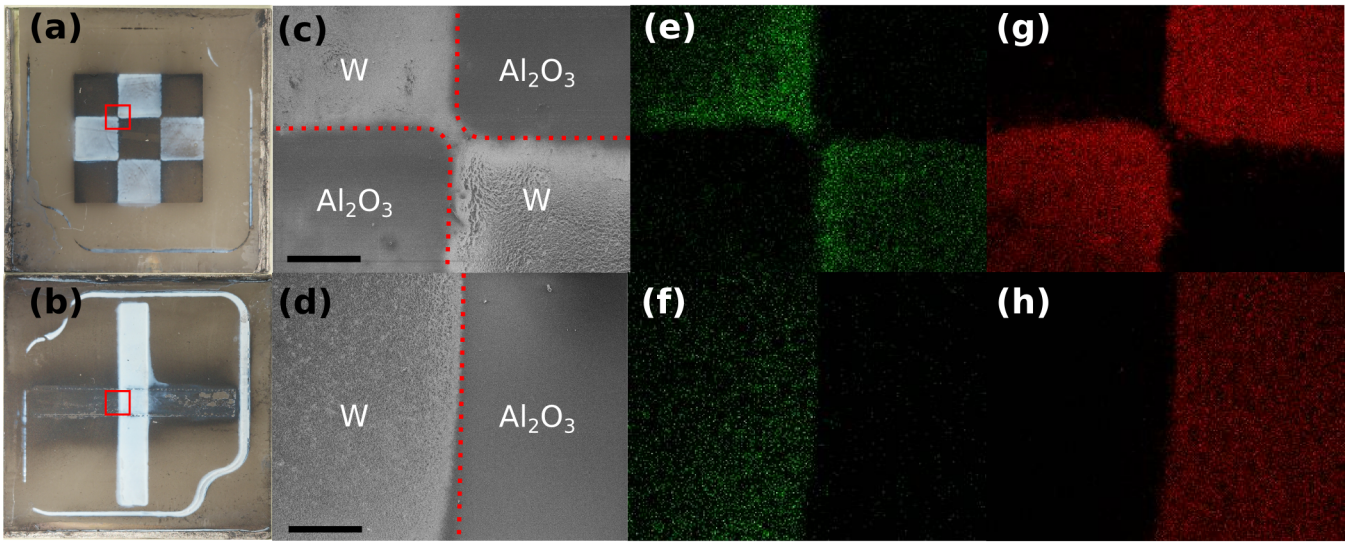

Figure 3: Multimaterial composite formed by light direct EPD. (a & b) Plane view images of the resulting composites. (a) Side-by-side deposition of tungsten (black) and alumina (white) particles in a checkerboard pattern while (b) demonstrates an alumina line intersecting and overtopping a tungsten line at a right angle. (c & d) Scanning electron micrographs of a region of the composite denoted approximately by a red square in (a) and (b), respectively. Dashed red lines indicate mask boundaries for the alumina mask level. Scale bars denote 500 microns. (e-h) Elemental maps acquired through energy-dispersive x-ray spectroscopy on the regions of interest in (c) & (d). (e & f) Elemental map of tungsten present in the region observed in (c) & (d), respectively. (g & h) Elemental map of aluminum present in the region observed in (c) & (d), respectively.

the zeta potential of the suspended particles were the same within measurement error both in the dark and under illumination with the mercury arc lamp, thus ruling out the possibility of increased mobility of the particles leading to the formation of the deposits. Therefore, the deposit is a result of electrophoretic deposition of particles onto a light actuated photoconductive electrode and not the result of thermal or electrothermal flows assembling the particles in the illuminated region. Below an illumination intensity of 6.4 mW cm^{-2} (broad band), no deposit was observed.

A series of feature size reproduction experiments were performed in which the mask consisted of rectangular slit 18.75 mm long and 0.25, 0.5, 1.25, 2.5, and 5 mm wide. The width of the resultant deposited features were measured under an optical microscope. Figure 2(b) plots the width of the deposited feature versus the width of the mask feature. Ideally, these data should lie on a line with a slope of one and an intercept of zero, representing perfect reproduction of the mask features. A linear regression of the data yields a slope of 1.00 ± 0.01 and an intercept of -0.024 ± 0.030 mm with an $R^2 = 0.999$, thus light-directed electrophoretic deposition faithfully reproduces features in this size range to within experimental error. Mask features below 250 microns could not be tested due to resolution limits of the laser cutter; however, inspection of the deposit boundary reveals that sub-resolution defects in the mask were reproduced. Thus, the ultimate resolution of the technique is likely less than 100 microns.

A representative photograph of a deposit patterned with the 2.5 mm mask is presented in Figure 2(c). Figure 2(d) presents a optical micrograph of the deposit. The cross sectional profile of a representative deposited strip with the 1.25 mm mask is presented in figure 2(d). In this case, the deposit is approximately 9 microns thick at the center and 14 microns thick at the edges. Notably, the deposit is thicker at the edges than in the center. This is a characteristic of deposits on electrode strips as observed by Pascall, *et al.*,[30] and, as they showed, is a result of a singularity in the electric field that results from a discontinuity in the electric boundary conditions at the edge of the electrode, or in this case, at the boundary between the illuminated and dark areas of the photoconductive electrode. This singularity leads to a high flux of particles to the edges where they accumulate to form the observed morphology.

Multimaterial light-directed electrophoretic deposition was demonstrated by depositing both tungsten and alumina nanoparticles in distinct locations on the photoconductive electrode to form a structured composite (**Figure 3**). In these experiments, the tungsten particles (black material) were deposited first. The tungsten

suspension was subsequently withdrawn and replaced with the alumina suspension which was then deposited. Specifically, figure 3(a) demonstrates the side-by-side placement of the two materials in a checkerboard pattern, while figure 3(b) demonstrates the ability to place one material on top of another. Both modes of material placement are required for fully 3D structured composites. Scanning electron micrographs of the regions denoted by the red square in figure 3(a) & (b) are shown in (c) & (d), respectively. The dashed red lines represents the location of the mask edge for the alumina layer.

Energy-dispersive x-ray spectroscopy (EDS) was performed on the resulting composites to determine the elemental compositions at various locations in the composite. Figure 3(e) & (f) show the presence of tungsten, while figure 3(g) & (h) show the presence of aluminum. These images clearly show the segregation of material into distinct locations that coincide with the illuminated regions during the deposition. It is interesting to note that a tungsten layer is confirmed to be present under the alumina layer by visual inspection of the underside of the photoconductive electrode, despite the lack of signal in the right half of figure 3(f). The thickness of the alumina layer significantly attenuates the x-ray signal from the tungsten layer.

We have presented a novel electrophoretic deposition technique based on using light to pattern materials on a photoconductive layer. This represents a large step in advancing electrophoretic deposition as a method of fabricating complex 3D patterned composites. Traditionally, composites formed with EPD have been limited to layering of materials normal to the electrode surface forming extruded 2D geometries due to the static nature of the deposition electrode. With light-directed electrophoretic deposition, we have demonstrated both the ability to pattern different materials in the plane of the electrode as well as place one material over another with high fidelity. The experiments presented utilized laser cut aluminum masks to define the illuminated regions and hence the lateral dimensions of the final deposit. This presents two limitations to the adoption of this technique for large scale additive manufacturing technique: a limit on the minimum feature size to 250 microns and the need to produce a physical mask for each deposited layer. While the first of these can be mitigated by moving to a higher resolution photomask, like those used in the semiconductor industry, the second provides more of a challenge. We believe the ultimate solution is to eliminate the physical mask altogether and instead utilize a digital projector to project a digital illumination pattern for each layer. Recently, such a light delivery system was utilized in a projection microstereolithography system and produced 10 micron lateral resolutions without any hard tooling.[36] By leveraging the wide materials set already demonstrated for traditional EPD, light-directed electrophoretic deposition can be viewed as new additive manufacturing technique that will allow for the fabrication of functional and graded 3D composites, including the ability to incorporate patterned void space through the use of a fugitive material that is removed through subsequent post-processing.

Supporting Information

Supporting Information is available online from the Wiley Online Library or from the author.

Acknowledgments

This work was funded by the Laboratory Directed Research and Development Strategic Initiative program 11-SI-005 and 14-SI-004 Funding support from DARPA Defense Sciences Office, Materials with Controlled Microstructural Architecture Program, Program Manager Dr. Judah Goldwasser, is gratefully acknowledged. We would also like to thank Dr. Klint Rose for initial discussions and Dr. Christian Grant for the profilometry data. This work was performed under the auspices of the US Department of Energy by Lawrence Livermore National Laboratory under Contract DE-AC52-07NA27344. LLNL-JRNL-644274.

References

[1] W. P. Davey, February 1919. United States Patent 1,294,627.

[2] L. Besra and M. Liu. *Prog. Mater. Sci.*, 52(1):1–61, January 2007.

[3] S. Yang, W. Cai, G. Liu, and H. Zeng. *J. Phys. Chem. C*, 113(18):7692–7696, May 2009.

[4] A. L. Rogach, N. A. Kotov, D. S. Koktysh, J. W. Ostrander, and G. A. Ragoisha. *Chem. Mater.*, 12(9):2721–2726, 2000.

[5] B. Neirinck, L. Van Mellaert, J. Fransaer, O. Van der Biest, J. Anné, and J. Vleugels. *Electrochem. Commun.*, 11(9):1842–1845, September 2009.

[6] W. Zhou, S. K. Watt, D. Tsai, V. T. Lee, and M. R. Zachariah. *J. Phys. Chem. B*, 117(6):1738–1745, February 2013.

[7] M. Ammam and J. Fransaer. *Sens. Actuators, B*, 160(1):1063–1069, December 2011.

[8] H. Hadraba, D. Drdlik, Z. Chlup, K. Maca, I. Dlouhy, and J. Cihlar. *J. Eur. Ceram. Soc.*, 33(12):2305–2312, October 2013.

[9] K. T. Sullivan, C. Zhu, D. J. Tanaka, J. D. Kuntz, E. B. Duoss, and A. E. Gash. *J. Phys. Chem. B*, 117(6):1686–1693, February 2013.

[10] G. Anné, K. Vanmeensel, J. Vleugels, and O. Van der Biest. *Key Eng. Mater.*, 314:213–218, 2006.

[11] O. Van der Biest, E. Joos, J. Vleugels, and B. Baufeld. *J. Mater. Sci.*, 41(24):8086–8092, 2006.

[12] A. R. Boccaccini, S. Keim, R. Ma, Y. Li, and I. Zhitomirsky. *J. R. Soc. Interface*, 7:S581–S613, May 2010.

[13] K. T. Sullivan, M. A. Worsley, J. D. Kuntz, and A. E. Gash. *Combust. Flame*, 159(6):2210–2218, June 2012.

[14] L. Tang, H. Feng, J. Cheng, and J. Li. *Chem. Commun.*, 46(32):5882–5884, August 2010.

[15] K. Zdansky and J. H. Dickerson. *Sens. Actuators, B*, 184:295–300, July 2013.

[16] T. Lu, L. Pan, H. Li, C. Nie, M. Zhu, and Z. Sun. *J. Electroanal. Chem.*, 661(1):270–273, October 2011.

[17] R. Hadar, D. Golodnitsky, H. Mazor, T. Ripenbein, G. Ardel, Z. Barkay, A. Gladkich, and E. Peled. *J. Phys. Chem. B*, 117(6):1577–1584, February 2013.

[18] D. Fu, X. L. Zhang, R. L. Barber, and U. Bach. *Adv. Mater.*, 22(38):4270–4274, 2010.

[19] W. Guo and B. Liu. *ACS Appl. Mater. Interfaces*, 4(12):7036–7042, December 2012.

[20] K. W. Song, R. Costi, and V. Bulović. *Adv. Mater.*, 25(10):1420–1423, March 2013.

[21] A. Nold, T. Assion, J. Zeiner, and R. Clasen. *Key Eng. Mater.*, 412:307–312, 2009.

[22] A. Nold, J. Zeiner, T. Assion, and R. Clasen. *J. Eur. Ceram. Soc.*, 30(5):1163–1170, March 2010.

[23] P. J. Pauzauskie, A. Jamshidi, J. K. Valley, J. H. Satcher, and M. C. Wu. *Appl. Phys. Lett.*, 95(11):113104, 2009.

[24] A. Jamshidi, S. L. Neale, K. Yu, P. J. Pauzauskie, P. J. Schuck, J. K. Valley, H. Hsu, A. T. Ohta, and M. C. Wu. *Nano Lett.*, 9(8):2921–2925, 2009.

[25] M. C. Wu. *Nat. Photonics*, 5(6):322–324, June 2011.

[26] S. J. Williams, A. Kumar, and S. T. Wereley. *Lab Chip*, 8(11):1879, 2008.

[27] R. C. Hayward, D. A. Saville, and I. A. Aksay. *Nature*, 404(6773):56–59, March 2000.

[28] W. D. Ristenpart, P. Jiang, M. A. Slowik, C. Punckt, D. A. Saville, and I. A. Aksay. *Langmuir*, 24(21):12172–12180, November 2008.

[29] M. Vaezi, S. Chianrabutra, B. Mellor, and S. Yang. *Virtual and Physical Prototyping*, 8(1):19–50, 2013.

[30] A. J. Pascall, K. T. Sullivan, and J. D. Kuntz. *J. Phys. Chem. B*, 117(6):1702–1707, February 2013.

[31] B. Liu and E. S. Aydil. *J. Am. Chem. Soc.*, 131(11):3985–3990, March 2009.

[32] H. Wang, G. Wang, Y. Ling, M. Lepert, C. Wang, J. Z. Zhang, and Y. Li. *Nanoscale*, 4(5):1463–1466, February 2012.

[33] A. Welte, C. Waldauf, C. Brabec, and P. J. Wellmann. *Thin Solid Films*, 516(20):7256–7259, August 2008.

[34] S. A. Hasan, D. W. Kavich, S. V. Mahajan, and J. H. Dickerson. *Thin Solid Films*, 517(8):2665–2669, February 2009.

[35] S. V. Mahajan and J. H. Dickerson. *Appl. Phys. Lett.*, 96(11):113105, March 2010.

[36] X. Zheng, J. Deotte, M. P. Alonso, G. R. Farquar, T. H. Weisgraber, S. Gemberling, H. Lee, N. Fang, and C. M. Spadaccini. *Rev. Sci. Instrum.*, 83(12):125001, December 2012.